Investigation of Aquo and Chloro Complexes of UO_2^{2+}, NpO_2^+, Np^{4+}, and Pu^{3+} by X-ray Absorption Fine Structure Spectroscopy

P. G. Allen,*,† J. J. Bucher,† D. K. Shuh,† N. M. Edelstein,† and T. Reich‡

Chemical Sciences Division, Lawrence Berkeley National Laboratory, Berkeley, California 94720, and Institute für Radiochemie, Forschungszentrum Rossendorf e. V., Postfach 51 01 19, D-01314 Dresden, Germany

Received May 1, 1997[⊗]

U, Np, and Pu $L_{II,III}$-edge X-ray absorption fine structure (XAFS) spectra were collected for the UO_2^{2+}, NpO_2^+, Np^{4+}, and Pu^{3+} ions as a function of chloride concentration in aqueous solution. At low chloride concentration, the hydration numbers and corresponding bond lengths for the different ions are as follows: UO_2^{2+}, $N = 5.3$, $R = 2.41$ Å; NpO_2^+, $N = 5.0$, $R = 2.50$ Å; Np^{4+}, $N = 11.2$, $R = 2.40$ Å; Pu^{3+}, $N = 10.2$, $R = 2.51$ Å. As the Cl^- concentration increases, inner-sphere Cl^- complexation occurs, resulting in a decrease in the hydration numbers and an expansion of the actinide−oxygen (water) bond lengths. The Pu^{3+} ion shows only a decrease in hydration number (40%) and no inner-sphere Cl^- complexation for $[Cl^-] < 14$ M. For concentrations up to 10−14 M Cl^-, the average Cl^- coordination numbers and bond lengths are as follows: UO_2^{2+}, $N = 2.6$, $R = 2.73$ Å; NpO_2^+, $N = 1.0$, $R = 2.84$ Å; Np^{4+}, $N = 2.0$, $R = 2.61$ Å. Structural changes are observed in the near-edge spectral region as shown by significant changes in the white line intensities upon Cl^- complexation. For ions with similar structures, i.e. Pu^{3+} and Np^{4+} or the actinyl ions NpO_2^+ and UO_2^{2+}, positive energy shifts are observed with increasing oxidation state. The ability to use XAFS speciation results to calculate equilibrium constants and the relationship of these results to previous studies are discussed.

Downloaded via LOS ALAMOS NATL LABORATORY on September 3, 2025 at 19:45:44 (UTC).
See https://pubs.acs.org/sharingguidelines for options on how to legitimately share published articles.

Introduction

Chloride complexation studies of the actinide ions Ac^{3+}, Ac^{4+}, AcO_2^+, and AcO_2^{2+} (Ac = U, Np, Pu) have been reported in several comprehensive reviews of thermodynamic data.[1−5] In general, these studies have employed a variety of analytical methods (solvent extraction, potentiometric titrations, ion exchange, etc.) to determine stability constants or, most frequently, stability quotients, which can be used in conjunction with extrapolation models (i.e., specific-ion interaction[6] or Pitzer[7]) to calculate the principal species in solution for a given set of ionic conditions. Not only is the identification of the chemical species important for understanding actinide separations and processing chemistry, but it also provides information which is essential for predicting actinide transport in the environment,[8] particularly with respect to the safety assessment of proposed nuclear waste repositories.

Although a large amount of work has been published, considerable discrepancies exist concerning the nature of the actinide−chloride interactions (inner-sphere or outer-sphere complexation), complex formation constants, and solution structure. Relatively good agreement is found for Cl^- complexation with the uranyl ion, UO_2^{2+}, where the log β_1 values for the formation of UO_2Cl^+ determined in 2 M (Cl^-, ClO_4^-) at 25 °C range from −0.06 to −0.15.[9−11] However, for NpO_2^+, a value of log $\beta_1 = -0.29$ has been reported,[12] while another study determined that no complexation occurs in this system.[13] More recently, a zero ionic strength value of −0.29 for log β_1 was obtained, and on the basis of spectroscopic evidence, the NpO_2Cl complex formation was proposed to be outer-sphere.[14] The log β_1 values obtained for Np(IV) in 2 M ClO_4^- solutions are also somewhat uncertain, ranging from +0.04 at 20 °C to −0.28 at 25 °C.[15,16] Other studies indicate that the species $NpCl^{3+}$ predominates in solutions of 5 M HCl.[17] The same types of discrepancies are also found for Pu(III), with log β_1 values reported from −0.15 to −2.43.[18,19]

† Lawrence Berkeley National Laboratory.
‡ Forschungszentrum Rossendorf e. v.
⊗ Abstract published in *Advance ACS Abstracts,* September 15, 1997.

(1) Grenthe, I.; Fuger, J.; Konings, R. J. M.; Lemire, R. J.; Muller, A. B.; Nguyen-Trung, C.; Wanner, H. In *Chemical Thermodynamics of Uranium*; Wanner, H., Forest, I., Eds.; Elsevier Science Publishers: Amsterdam, 1992; p 193.
(2) Ahrland, S. In *The Chemistry of the Actinide Elements, Vol. 2*; Katz, J. J., Seaborg, G. T., Morss, L. R., Eds.; Chapman and Hall: New York, 1986; p 1498.
(3) Fuger, J. In *Plutonium Chemistry*; Carnall, W. T., Choppin, G. R., Eds.; ACS Symposium Series 216; American Chemical Society: Washington DC, 1983; p 74.
(4) Degischer, G.; Choppin, G. R. in *Gmelin Handbuch der Anorganische Chemie, Transuranium*; Springer-Verlag: Berlin, 1975; Part D1, Suppl. Vol. 20, p 129.
(5) (a) Sillén, L. G.; Martell, A. E. *Stability Constants of Metal-Ion Complexes*; Special Publication No. 17; The Chemical Society: London, 1964. (b) Sillén, L. G.; Martell, A. E. *Stability Constants of Metal-Ion Complexes*; Special Publication No. 25; The Chemical Society: London, 1971.
(6) (a) Scatchard, G. *Chem. Rev.* **1936**, *19*, 309. (b) Ciavatta, L. *Ann. Chim.* (*Rome*) **1980**, 551.
(7) Pitzer, K. S. in *Activity Coefficients in Electrolyte Solutions*; Pitzer, K. S., Ed.; CRC Press: Boca Raton, FL, 1991; p 75.
(8) (a) Chemistry and Migration Behaviour of Actinides and Fission Products in the Geosphere: Proceedings of the Fourth International Conference, Charleston, SC, 1993. *Radiochim. Acta* **1994**, *66/67*, 1. (b) Chemistry and Migration Behaviour of Actinides and Fission Products in the Geosphere: Proceedings of the Fifth International Conference, Saint Malo, France, 1995. *Radiochim. Acta* **1996**, *74*, 1.
(9) Day, R. A.; Powers, R. M. *J. Am. Chem. Soc.* **1954**, *76*, 3895.
(10) Bednarczyk, L.; Fidelis, I. *J. Radioanal. Nucl. Chem.* **1978**, *45*, 325.
(11) Awasthi, S. P.; Sundaresan, M. *Indian J. Chem.* **1981**, *20A*, 378.
(12) Gainar, I.; Sykes, K. W. *J. Chem. Soc.* **1964**, 4452.
(13) Danesi, P. R.; Chiarizia, R.; Scibona, G.; D'Alessandro, G. *J. Inorg. Nucl. Chem.* **1974**, *36*, 2396.
(14) Neck, V.; Fanghänel, Th.; Rudolph, G.; Kim, J. I. *Radiochim. Acta* **1995**, *69*, 39.
(15) Shilin, I. V.; Nazarov, V. K. *Radiokhimiya* **1966**, *8*, 514.
(16) Sykes, K. W.; Taylor, B. L. *Proc. Int. Conf. Coord. Chem.* **1962**, *7*, 31.
(17) Marcus Y. *Coord. Chem. Rev.* **1967**, *2*, 195.
(18) Connick, R. E.; McVey, W. H. *J. Am. Chem. Soc.* **1953**, *75*, 474.
(19) Shiloh, M.; Marcus, Y. *J. Inorg. Nucl. Chem.* **1966**, *28*, 2725.

S0020-1669(97)00502-8 CCC: $14.00 © 1997 American Chemical Society

These data indicate that chloride complexation with the actinide ions UO_2^{2+}, NpO_2^{+}, Np^{4+}, and Pu^{3+} is extremely weak. Since most of the research to date has been based on indirect analytical methods, the structures as well as the actual existence of these complexes in high ionic strength brines have not been directly confirmed. We have investigated the formation of chloride complexes with the actinide ions UO_2^{2+}, NpO_2^{+}, Np^{4+}, and Pu^{3+} using X-ray absorption fine structure (XAFS) spectroscopy.[20] These species were chosen as representatives of the AcO_2^{2+}, AcO_2^{+}, Ac^{4+}, and Ac^{3+} ions because of their availability and stability. In this paper, the Cl^- concentration in aqueous solution is systematically varied, and XAFS is used to determine the structural changes that occur around the actinide core ion. Since XAFS spectroscopy directly determines the local structural environment for metal ions in solution, actinide chloro and aquo complexes that have been postulated in earlier work can be directly characterized.

Experimental Section

Solution and Sample Preparation. All sample preparations were done using the Actinide Chemistry Group facilities at the Lawrence Berkeley National Laboratory (LBNL). ACS reagent grade anhydrous lithium chloride (Aldrich) and ACS reagent grade concentrated hydrochloric acid (J. T. Baker) were used as received. Analytical grade Dowex anion exchange resin, AG1-X8, 200−400 mesh, chloride form (Bio-Rad), with 3.2 mequiv/g of resin exchange capacity was used. The resin was washed with a series of 1, 6, and 9 M HCl solutions until the eluant was clear. A final rinse with 0.1 M HCl was made before the resin was filtered to remove the excess liquid. Double-distilled deionized water was used for all solution preparations.

A 2.0 M stock solution of the UO_2^{2+} ion was prepared from uranyl nitrate, $UO_2(NO_3)_2{\cdot}6H_2O$ (B & A, Allied Chemical & Dye Corp.). All lithium chloride solutions were prepared from a 0.001 M HCl solution. A 0.46 M stock solution of NpO_2^{+} was prepared by dissolving NpO_2 powder (^{237}Np) obtained from Los Alamos National Laboratory in 0.100 M HCl. The isotopic purity was determined by high-resolution α spectroscopy using a surface barrier detector (Tennelec, ∼20 keV resolution). In addition to ^{237}Np, the stock solution contained 0.26 mol % ^{239}Pu and 0.0003 mol % ^{241}Am. Stock solution concentrations were determined by comparing a 1:2000 dilution ^{237}Np platinum counting plate against an ^{241}Am standard (traceable to NBS). A plot of the apparent ^{237}Np concentration versus ^{241}Am counting efficiency was made to allow extrapolation to "zero" efficiency in order to correct for the different geometries of isotope deposition on the counting plates.

Removal of the ^{239}Pu, ^{241}Am impurities, and the equilibrium ^{233}Pa daughter was accomplished by multiple extractions using 0.5 M TTA (thenoyltrifluoroacetone) in benzene followed by several benzene washes to remove the residual TTA. α spectroscopy confirmed the removal of ^{239}Pu (which interferes with the Np XAFS data collection) and ^{241}Am to detection limits. A 0.1 M stock solution of the Np^{4+} ion was prepared from the NpO_2^{+} solution by reduction to Np^{3+} using a Zn amalgam followed by air oxidation to Np^{4+}. The stock was maintained at 0.1 M HCl acidity. Similarly, a 0.035 M Pu^{3+} stock solution was prepared from a Pu^{4+} solution by Zn amalgam reduction. The plutonium isotope used was ^{242}Pu, and the principal transuranic impurity was ^{241}Am (0.05 mol %).

Most of the solutions were mixed in 10 mm diameter plastic centrifuge tubes in an ambient-atmosphere glovebox. The final actinide and chloride concentrations are summarized in Table 1. LiCl was used in the NpO_2^{+} solution preparations to avoid disproportionation and in the UO_2^{2+} and Pu^{3+} solutions when higher Cl^- activities were desired. The LiCl solutions of UO_2^{2+}, NpO_2^{+}, and Pu^{3+} were kept at pH = 2, 3, and 3, respectively, to avoid hydrolysis reactions. Smaller plastic tubes (5 mm diameter) and sample volumes were used at high chloride concentrations to minimize the attenuation and background scattering from the Cl^- ions in the solutions. The Dowex resin samples were prepared by allowing the mixture to equilibrate and removing most of the residual solution, leaving a wet paste. The solutions were sealed in the tubes by melting the caps directly onto the plastic body with a soldering iron. The outsides of the samples were surveyed to ensure that no detectable α radiation was present. With the integrity of the primary containers established, each sample was placed within two additional layers of containment consisting of two heat-sealed polyethylene bags. The triply contained, inspected, and certified samples were then transported to the Stanford Synchrotron Radiation Laboratory (SSRL). The samples (5−10 at any given time) were mounted on an aluminum frame which was placed inside a quaternary containment box with 0.17 mm polycarbonate X-ray windows. The box was placed inside the X-ray hutch on a specially designed sample positioner. The hutch, as well as the sample mounting and storage areas, was equipped with LBNL continuous air monitors, α radiation detectors, and alarms for safety purposes. Access to the samples was carefully controlled at all times.

Table 1. Summary of Solution Preparations

actinide ion	$[Ac^{x+}]^a$	medium	$[Cl^-]^a$	path length (mm)	mode[b]
UO_2^{2+}	0.1	H_2O	0.0	10	T
	0.1	HCl	1.0	10	T
	0.1	HCl	2.0	10	T
	0.1	HCl	4.0	10	T
	0.1	HCl	6.0	10	T
	0.1	HCl	8.0	10	T
	0.1	HCl	10.0	10	T
	0.04	LiCl	12.0	5	F
	0.04	LiCl	14.0	5	F
	0.02	Dowex/HCl	10.0	10	F
NpO_2^{+}	0.005	LiCl	3.0	10	F
	0.005	LiCl	4.0	10	F
	0.005	LiCl	5.0	10	F
	0.005	LiCl	6.0	10	F
	0.005	LiCl	7.0	10	F
	0.005	LiCl	8.0	10	F
	0.005	LiCl	9.0	10	F
	0.005	LiCl	10.0	10	F
Np^{4+}	0.005	HCl	1.0	10	F
	0.005	HCl	2.0	10	F
	0.005	HCl	3.0	10	F
	0.005	HCl	4.0	10	F
	0.005	HCl	5.0	10	F
	0.005	HCl	6.0	10	F
	0.005	HCl	8.0	10	F
	0.005	HCl	10.0	10	F
	0.005	Dowex/HCl	10.0	10	F
Pu^{3+}	0.020	LiCl	0.01	10	F
	0.004	LiCl	7.0	5	F
	0.004	LiCl	8.7	5	F
	0.004	LiCl	10.5	5	F
	0.004	LiCl	12.3	5	F

[a] Molar concentration in units of mol·dm^{-3}. [b] Samples were measured in the transmission (T) or fluorescence (F) mode.

XAFS Data Acquisition and Analysis. Uranium, neptunium, and plutonium $L_{II,III}$ edge X-ray absorption spectra were collected at SSRL on wiggler beamline 4-1 under normal ring operating conditions (3.0 GeV, 50−100 mA). Energy scans of the polychromatic X-ray beam were obtained using a Si(220) double-crystal monochromator. The vertical slit width was 0.5 mm, which reduces the effects of beam instabilities and monochromator glitches while providing ample photon flux. The higher order harmonic content of the beam was rejected by detuning the crystals in the monochromator so that the incident flux was reduced to 50% of its maximum at the scan ending energy. The samples containing UO_2^{2+} in 1−10 M HCl and the UO_2^{2+}/Dowex sample were measured in the transmission mode using Ar-filled ionization chambers. All of the neptunium, plutonium, and the remaining uranium solutions were measured in the fluorescence mode using a Ge solid state detector developed at Lawrence Berkeley National Laboratory.[21] The detector was operated at ∼200 kHz per channel, and the spectra were corrected for detector deadtime using a 2 μs time constant.

(20) Prins, R.; Koningsberger, D. E. *X-ray Absorption: Principles, Applications, Techniques for EXAFS, SEXAFS, and XANES*; Wiley-Interscience: New York, 1988.

(21) Bucher, J. J.; Edelstein, N. M.; Osborne, K. P.; Shuh, D. K.; Madden, N.; Luke, P.; Pehl, D.; Cork, C.; Malone, D.; Allen, P. G. SRI '95 Conference Proceedings. *Rev. Sci. Instr.* **1996**, *67*, 1.

XAFS data reduction, including treatment of both the extended X-ray absorption fine structure (EXAFS) and the X-ray absorption near-edge structure (XANES) spectral regions, was performed by standard methods reviewed elsewhere[20] using the suite of programs EXAFSPAK developed by G. George of SSRL. Typically, three XAFS scans (transmission or fluorescence) were collected from each sample at ambient temperature (~25 °C) and the results were averaged. The spectra were energy-calibrated by simultaneously measuring the absorption spectrum for the reference sample UO_2, NpO_2, or PuO_2 as appropriate. The energies of the first inflection points for the reference sample absorption edges, E_r, were defined at 17 166.0 eV (U L_{III}), 17 606.2 eV (Np L_{III}), and 22 258.0 (Pu L_{II}). Pu XAFS data were acquired at the L_{II}-edge to avoid monochromator crystal glitches encountered at $k = 8$ Å^{-1} above the L_{III}-edge. The EXAFS threshold energies, E_0, were defined as 17 185, 17 625, and 22 275 eV for the U, Np, and Pu samples, respectively. Nonlinear least-squares curve fitting for the raw k^3-weighted EXAFS data and spectral deconvolutions of the XANES data were done using the EXAFSPAK programs.

The EXAFS data were fit using theoretical phases and amplitudes calculated from the program FEFF6 of Rehr *et al.*[22] All of the interactions were modeled using single scattering (SS) and multiple scattering paths (MS) derived from the model compounds $UO_2Cl_2 \cdot H_2O$,[23] $CsNpO_2Cl_2 \cdot H_2O$,[24] and Cs_2UCl_6 (i.e., $NpCl_6^{2-}$ or $PuCl_6^{2-}$)[25] and the hypothetical clusters $Np(H_2O)_{12}^{4+}$ and $Pu(H_2O)_{10}^{3+}$. For the actinyl complex spectra, a total of four paths were employed: SS Ac−O_{ax} (axial), SS Ac−O_{eq} (equatorial), SS Ac−Cl, and MS O−Ac−O (four-legged path). Since the MS path occurs at exactly twice the Ac−O_{ax} distance, it is included as a fixed parameter directly linked to the floating Ac−O_{ax} parameters.[26,27] Fits to the Np^{4+} and Pu^{3+} data utilized two paths: SS Ac−O and SS Ac−Cl. An initial series of fits were done on the UO_2^{2+}/0.0 M HCl and the UO_2^{2+}/Dowex data to establish accurate Debye-Waller factors, σ, for the Ac−O_{eq} and Ac−Cl shells. Similarly, reasonable values of σ were obtained for the Np^{4+} O and Cl^- interactions using the Np^{4+}/1.0 M HCl and Np^{4+}/Dowex data. All the subsequent fits were performed using fixed σ values for these shells, and a fixed coordination number of $N = 2$ for the Ac−O_{ax} shell. S_0^2, the amplitude reduction factor, was held fixed at 0.9 in each of the fits. The shift in threshold energy, ΔE_0, was allowed to vary as a global parameter in each of the fits (i.e., the same ΔE_0 was used for each shell). Consequently, the fits were highly constrained, which avoided N and σ correlation problems and established more consistently the changes in coordination as a function of Cl^- concentration.[28,29]

Results and Discussion

UO_2^{2+} EXAFS. Figure 1 shows the raw k^3-weighted EXAFS data and the corresponding Fourier transforms (FT) for UO_2^{2+} in aqueous solution as a function of chloride concentration. The theoretical curve fits are also shown, and the structural results are summarized in Table 2. The FT represents a pseudoradial distribution function, and the peaks are shifted to lower R values as a result of the phase shifts associated with the absorber−scatterer interactions (~0.2−0.5 Å). In the absence of Cl^-, the FT of the free uranyl spectrum shows two peaks which arise from the presence of 2 O_{ax} at 1.76 Å and ~5 O_{eq} at 2.41 Å. This is consistent with the structural results obtained previously for the fully hydrated uranyl ion.[30,31] The spectrum of the UO_2^{2+}/Dowex sample shows a different pattern with a much larger FT peak occurring at a higher R value than the O_{eq} peak for the hydrated uranyl ion. The curve fits indicate that the complex anion $UO_2Cl_4^{2-}$, analogous to that in $Cs_2UO_2Cl_4$ solid,[32] is formed in the Dowex resin with 4.2 Cl^- at 2.67 Å. Although the Dowex FT displays a peak occurring in the same region as the O_{eq} peak in the hydrated uranyl FT, the curve fits show no evidence for O_{eq} (no improvement in the fit by including O_{eq}). The spurious peak at 1.7 Å in the Dowex FT is a side lobe arising from truncation effects[20] and illustrates one of the difficulties in making FT assignments without performing detailed curve fits. An inspection of the 1−14 M Cl^- data shows that a structural transformation is occurring in the equatorial region, and initial curve fits to these spectra indicated the structural changes could be fit primarily by changes

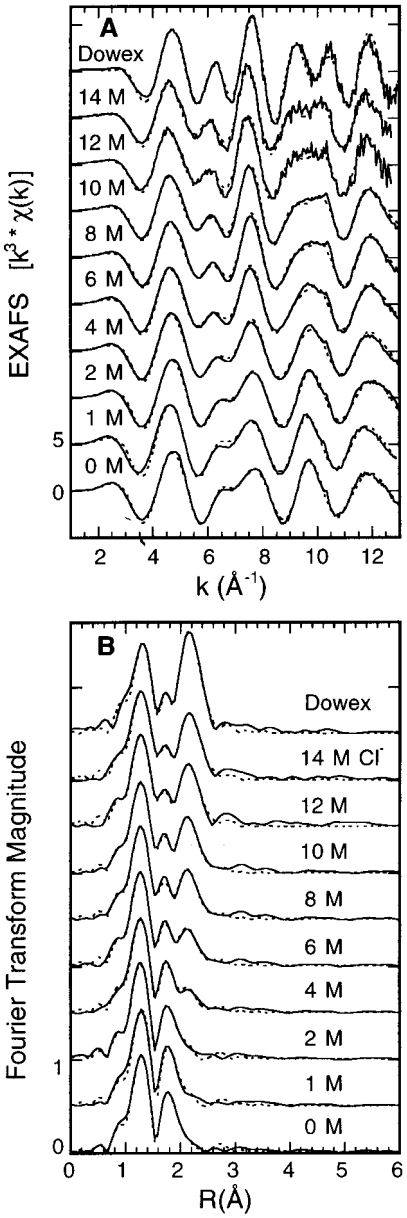


Figure 1. Raw U L_{III}-edge k^3-weighted EXAFS data (A) and corresponding Fourier transforms (B) taken over $k = 1-13$ Å^{-1} for UO_2^{2+} as a function of [Cl^-] and the UO_2^{2+}/Dowex reference: experimental data (—); theoretical fit (···).

(22) Rehr, J. J.; Mustre de Leon, J.; Zabinsky, S.; Albers, R. C. *Phys. Rev. B* **1991**, *44*, 4146.
(23) Taylor, J. C.; Wilson, P. W. *Acta Crystallogr.* **1974** *B30*, 169.
(24) Tomilin, S. V.; Yu, F.; Volkov, F.; Melkaya, R. F.; Spiryakov, V. I.; Kapshukov, I. I. *Sov. Radiochem.* (*Engl. Transl.*) **1986**, *28*, 634.
(25) Schleid, T.; Meyer, G.; Morss, L. R. *J. Less-Common Met.* **1972**, *132*, 69.
(26) Allen, P. G.; Bucher, J. J.; Clark, D. L.; Edelstein, N. M.; Ekberg, S. A.; Gohdes, J. W.; Hudson, E. A.; Kaltsoyannis, N.; Lukens, W. W.; Neu, M. P.; Palmer, P. D.; Reich. T.; Shuh, D. K.; Tait, C. D.; Zwick, B. D. *Inorg. Chem.* **1995**, *34*, 4797.
(27) Allen, P. G.; Shuh, D. K.; Bucher, J. J.; Edelstein, N. M.; Reich. T.; Denecke, M. A.; Nitsche, H. *Inorg. Chem.* **1996**, *35*, 784.
(28) Allen, P. G.; Conradson, S. D.; Wilson, M.; Gottesfeld, S.; Raistrick, I. D.; Valerio, J.; Lovato, M. *Electrochim. Acta* **1994**, *39*, 2415.
(29) Allen, P. G.; Conradson, S. D.; Wilson, M.; Gottesfeld, S.; Raistrick, I. D.; Valerio, J.; Lovato, M. *J. Electroanal. Chem. Interfacial Electrochem.* **1995**, *384*, 99.
(30) Åberg, M.; Ferri, D.; Glaser, J.; Grenthe, I. *Inorg. Chem.* **1983**, *22*, 3986.
(31) Thompson, H. A.; Brown, G. E., Jr.; Parks, G. A. *Am. Mineral.* **1997**, *82*, 483.
(32) Hall, D.; Rae, A. D.; Waters, T. N. *Acta Crystallogr.* **1966**, *20*, 160.

Table 2. EXAFS Structural Parameters for UO_2^{2+} Chloride Solutions[a]

sample UO_2^{2+}	U−O_{ax}			U−O_{eq}		U−Cl			
	R (Å)	N[b]	σ^2 (Å^2)[c]	R (Å)	N	R (Å)	N	ΔE_0 (eV)	F ratio
0 M HCl	1.76	2	0.0018	2.41	5.3			−10.2	1.0
1 M HCl	1.76	2	0.0016	2.41	5.0	2.71	0.3	−10.8	0.87
2 M HCl	1.75	2	0.0016	2.41	4.8	2.72	0.4	−12.2	0.75
4 M HCl	1.76	2	0.0017	2.41	3.9	2.71	1.0	−11.7	0.43
6 M HCl	1.76	2	0.0015	2.44	3.1	2.72	1.5	−11.5	
8 M HCl	1.76	2	0.0015	2.48	2.7	2.73	1.8	−10.8	
10 M HCl	1.76	2	0.0016	2.50	2.5	2.73	2.0	−10.7	
12 M LiCl	1.77	2	0.0015	2.51	2.2	2.73	2.2	−10.4	
14 M LiCl	1.77	2	0.0018	2.52	1.9	2.73	2.6	−9.6	
Dowex/HCl	1.76	2	0.0022			2.67	4.2	−12.3	1.0
$[UO_2(H_2O)_x^{2+}]$[d]	1.70	2		2.42	4.9				
$[UO_2(H_2O)_x^{2+}]$[e]	1.77	2		2.42	5.0				
$UO_2Cl_2{\cdot}H_2O$[f]	1.72	2		2.46	1	2.78	4		
$Cs_2UO_2Cl_4$[g]	1.81	2				2.62	4		

[a] The 95% confidence limits for R and N as estimated by EXAFSPAK: U−O_{ax}, $R \pm 0.006$ Å; U−O_{eq}, $R \pm 0.012$ Å and $N \pm 0.30$; U−Cl, $R \pm 0.012$ Å and $N \pm 0.30$, respectively. [b] $N = 2$, held constant for the U−O_{ax} shell. [c] σ^2 = Debye−Waller factor squared held constant for the additional shells; U−O_{eq}, $\sigma^2 = 0.0070$; U−Cl, $\sigma^2 = 0.0050$. [d] XRD; ref 30. [e] EXAFS; ref 31. [f] XRD; ref 23. [g] XRD; ref 32.

in the O_{eq} and Cl^- coordination numbers. Therefore, in subsequent fits, the values of σ for the O_{eq} and Cl^- shells were fixed to those obtained from the $UO_2(H_2O)_5^{2+}$ and $UO_2Cl_4^{2-}$ spectra.

From 1 to14 M Cl^-, the curve fits demonstrate a systematic replacement of O_{eq} by Cl^-. As the Cl^- concentration increases, the Cl^- coordination number N_{Cl^-} increases from 0.3 to 2.6, the O_{eq} coordination number $N_{O_{eq}}$ decreases from 5.0 to 1.9, and bond lengths for the O_{eq} shell lengthen from 2.41 to 2.52 Å. It is important to note that the curve-fitting results represent an average of all possible species present in these solutions, i.e., $UO_2(H_2O)_5^{2+}$, $UO_2(H_2O)_xCl^+$, or $UO_2(H_2O)_xCl_2$. The 95% confidence limits for R and N and the F value ratios obtained from the end point fits are also shown in Table 2.[33] On the basis of these results, the presence of Cl^- at 4 M is confirmed. However, the confidence limits show that this is not the case for the 1 and 2 M spectra. While it appears that there is a trend in the F ratios, and an increase in precision gained by measuring multiple spectra in EXAFS has been demonstrated,[28,29] the fitting results of $\sim 0.3 \pm 0.3$ Cl^- obtained by the inclusion of Cl^- in the 1 and 2 M data are at the noise level. One of the important results obtained is the presence of 2.6 ± 0.3 Cl^- in 14 M Cl^-. A value of $N_{Cl^-} > 2$, even with the effects of averaging, necessitates the presence of a species having the form $UO_2(H_2O)_xCl_3^-$. These data also suggest that as the molar ratio of H_2O/UO_2^{2+} decreases, the concomitant decrease in N_{Oeq} is mitigated through simple Cl^- replacement—an effect which at this level is indistinguishable from that of a decrease in the activity of H_2O.[30] The structural effect of Cl^- replacement is to lengthen the U−O_{eq} bonds.

NpO_2^+ EXAFS. The raw k^3-weighted EXAFS data and Fourier transforms for NpO_2^+ are shown in Figure 2 along with the corresponding fits as a function of the Cl^- concentration. Although there is a higher noise level in these data acquired in the fluorescence mode relative to the uranyl spectra measured in the transmission mode, the important features are clearly observed in the FTs. The FT for NpO_2^+ in 3 M Cl^- shows two peaks analogous to the O_{ax} and O_{eq} peaks for UO_2^{2+} without Cl^-. As the Cl^- concentration is increased from 6 to 10 M, an additional peak appears immediately to the high R side of the O_{eq} peak. This peak correlates in both position and magnitude to the Cl^- peak for UO_2^{2+} in 4 M Cl^-. Spectral changes are observed in the k-space data in Figure 2a around $k = 6-7$ Å^{-1} (also see Figure 1a). Since the NpO_2^+ ion has a structure similar

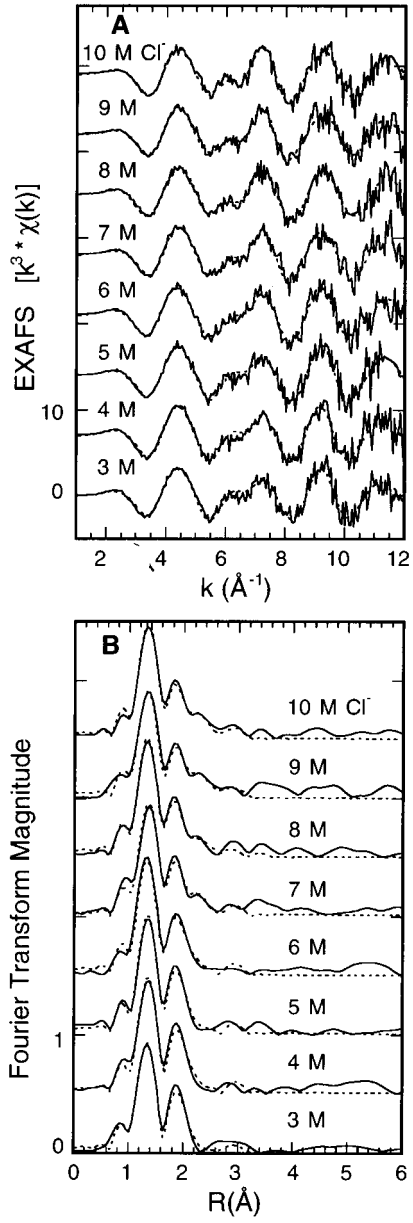


Figure 2. Raw Np L_{III}-edge k^3-weighted EXAFS data (A) and corresponding Fourier transforms (B) taken over $k = 1-12$ Å^{-1} for NpO_2^+ as a function of [Cl^-]: experimental data (—); theoretical fit (···).

(33) F is a goodness of fit parameter defined as $F = \Sigma k^6(\text{data} - \text{fit})^2/(N_{pts} - N_{var})$ where N_{pts} is the number of data points and N_{var} is the number of floating variables. The ratio of F values obtained with and without the inclusion of a Cl^- (or O) shell of atoms is used here to quantify the fit improvement with Cl^- (or O) in the end point spectra (i.e., Cl^- detection limits in 0, 1, 2, and 4 M HCl and O detection limits in the Dowex sample).

Table 3. EXAFS Structural Parameters for NpO_2^+ Chloride Solutions[a]

sample NpO_2^+	Np−O_{ax}			Np−O_{eq}		Np−Cl			
	R (Å)	N[b]	σ^2 (Å^2)[c]	R (Å)	N	R (Å)	N	ΔE_0 (eV)	F ratio
3 M LiCl	1.85	2	0.0018	2.50	5.0			−6.7	1.0
4 M LiCl	1.85	2	0.0012	2.52	5.3			−7.0	1.0
5 M LiCl	1.84	2	0.0010	2.51	5.1			−7.7	0.95
6 M LiCl	1.83	2	0.0015	2.52	5.0			−8.5	1.0
7 M LiCl	1.85	2	0.0013	2.53	4.0	2.84	0.7	−7.1	0.37
8 M LiCl	1.84	2	0.0012	2.53	4.0	2.83	0.6	−8.6	0.56
9 M LiCl	1.84	2	0.0018	2.54	3.9	2.85	1.0	−6.9	0.38
10 M LiCl	1.84	2	0.0012	2.53	4.1	2.84	1.0	−6.8	0.34
$[NpO_2(H_2O)_x^+]$[d]	1.83	1.6		2.52	5.2				
$CsNpO_2Cl_2 \cdot H_2O$[e]	1.81	2		2.49	1	2.86	4		

[a] The 95% confidence limits as estimated by EXAFSPAK: Np-O_{ax}, $R \pm 0.009$ Å; Np−O_{eq}, $R \pm 0.020$ Å and $N \pm 1.0$; Np−Cl, $R \pm 0.039$ Å and $N \pm 0.45$. [b] $N = 2$, held constant for the Np−O_{ax} shell. [c] Debye−Waller factor held constant for the additional shells; Np−O_{eq}, $\sigma^2 = 0.0070$; Np−Cl, $\sigma^2 = 0.0050$. [d] EXAFS; ref 34. [e] XRD; ref 24.

to that of UO_2^{2+}, curve fits were done using the same σ values for the O_{eq} and Cl^- shells that were used in the UO_2^{2+} fits (Table 3).

In 3 M Cl^-, the Np(V) environment consists of 2 O_{ax} at 1.85 Å and 5 O_{eq} at 2.50 Å.[34] This structure is nearly identical to that of the fully hydrated UO_2^{2+} ion with the exception of longer bond lengths which are expected for the larger Np(V) ion. For higher Cl^- concentration, N_{Cl^-} increases from 0 to ∼1, $N_{O_{eq}}$ decreases from ∼5 to 4, and the O_{eq} bond lengths expand from 2.50 to 2.53 Å. As was done for the fits to the uranyl EXAFS, F value ratios were determined along with 95% confidence limits for R and N. However, since the NpO_2^+ EXAFS data possess a significant amount of high-frequency noise, the F value ratios reported were derived from fits to Fourier-filtered data to remove the noise.[35] The factor of 2 improvement achieved by including Cl^- in the fits of the 7−10 M Cl^- spectra shows that Cl^- is present in the equatorial region of the NpO_2^+ ion for these solutions. The relative magnitudes and positions of the different contributions to the fit of the 10 M spectrum are shown in Figure 3 for comparison. Although the uncertainty in N_{Cl^-} is relatively large, the Np−O_{eq} and Np−Cl bond lengths are in agreement with those reported by XRD for the solid $CsNpO_2Cl_2 \cdot H_2O$.[24] These data show that the Cl^- replacement in NpO_2^+ is substantially weaker than that in UO_2^{2+}, yet the nature of the complexation is the same (i.e., the water molecules move out, and the Cl^- ligation is inner-sphere).

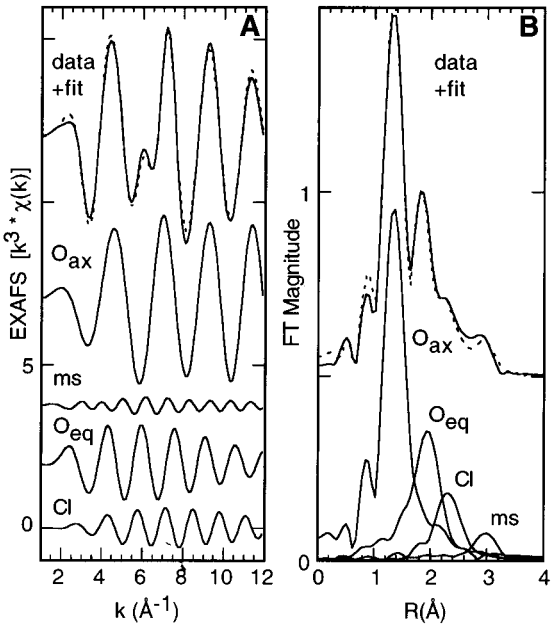


Figure 3. Curve-fit deconvolution in k-space (A) and R-space (B) for a fit to the Fourier-filtered EXAFS data for NpO_2^+ in 10 M LiCl. The contributions are Np−O_{ax} (63%), O−Np−O (MS, 5%), Np−O_{eq} (19%), and Np−Cl (13%).

Np^{4+} EXAFS. Figure 4 shows the raw k^3-weighted EXAFS data and the corresponding FTs for Np^{4+} as a function of chloride concentration. The curve-fitting results are summarized in Table 4. The FT for Np^{4+} in 1 M Cl^- shows a single prominent peak which is fit by a single shell of ∼11 O at 2.40 Å. Although the hydration number typically assigned for tetravalent actinides is ∼8,[36] there have been relatively few direct studies and the results cover a range of values. For Th^{4+}, an XRD study found ∼8 water molecules at 2.49 Å[37] while an NMR measurement has reported a hydration number of 10.[38] XRD determined the environment around U^{4+} to contain ∼9 water molecules at 2.51 Å.[39] The O coordination number determined by EXAFS suffers from at least a 10% uncertainty, making it impossible to distinguish between hydration numbers of 10 and 12 at the 95% confidence level. However, the Np−O bond length in $Np(H_2O)_{11}^{4+}$ agrees with the average Pu−O bond length of 2.41 Å in the complex $Pu(NO_3)_2(H_2O)_x^{2+}$, which was estimated to be 11-coordinate on the basis of EXAFS amplitude comparisons with the 12-coordinate species $Pu(NO_3)_6^{2-}$.[40] That these bond lengths are longer than the 2.35 Å value[41] for 8-coordinate Np in NpO_2 and shorter than the 2.51 Å value[42] for Np in 12-coordinate $Np(NO_3)_6^{2-}$ suggests that the number of waters around the Np^{4+} ion lies in the range of 9−11.

The spectrum of the Np^{4+}/Dowex sample yields a much larger FT peak occurring at a higher R value than the O peak in the 1 M spectrum. Curve fitting yields ∼6 Cl^- at 2.61 Å, suggesting that the complex anion $NpCl_6^{2-}$ is formed in the Dowex resin. This structure and the bond lengths agree with those found previously for the octahedral $AcCl_6^{2-}$ units present in Cs_2UCl_6[25] and Cs_2PuCl_6.[43] The FTs in Figure 4b show that there are no structural changes occurring up to 5−6 M Cl^-, whereas from 6 to 10 M Cl^-, there is a clear shift to higher R

(34) Combes, J. M.; Chisholm-Brause, C. J.; Brown, G. E., Jr.; Parks, G. A.; Conradson, S. D.; Eller, P. G.; Triay, I. R.; Hobart, D. E.; Meijer, A. *Environ. Sci. Technol.* **1992**, *26*, 376.
(35) The data were Fourier-filtered over the ranges $k = 1-12$ Å^{-1} and $R = 0.2-3.2$ Å, and the filtered fits gave results that were nearly identical to those obtained from the raw data fits. The value for N_{pts} used to calculate the F values is estimated by $2\,\Delta k\,\Delta R/\pi$.
(36) Choppin, G. R. *Radiochim. Acta* **1983**, *32*, 43.
(37) Johansson, G.; Magini, M.; Ohtaki, H. *J. Solution Chem.* **1991**, *20*, 775.
(38) Fiat, D.; Connick, R. E. *J. Am. Chem. Soc.* **1966**, *88*, 4754.
(39) Pocev, S.; Johansson, G. *Acta Chem. Scand.* **1973**, *27*, 2146.
(40) Allen, P. G.; Veirs, D. K.; Conradson, S. D.; Smith, C. A.; Marsh, S. F. *Inorg. Chem.* **1996**, *35*, 2841.
(41) Zachariasen, W. H. Natl. Nuclear Energy Ser., Div. IV **1949**, *14B*, Transuranium Elements, Pt. II, 1489.
(42) (a) Grigor'ev, M. S.; Gulev, B. F.; Krot, N. N. *Radiokhimiya* **1986**, *28*, 685. (b) Grigor'ev, M. S.; Yanovskii, A. I.; Krot, N. N. *Radiokhimiya* **1987**, *29*, 574.
(43) Zachariasen, W. H. *Acta Crystallogr.* **1948**, *1*, 268.

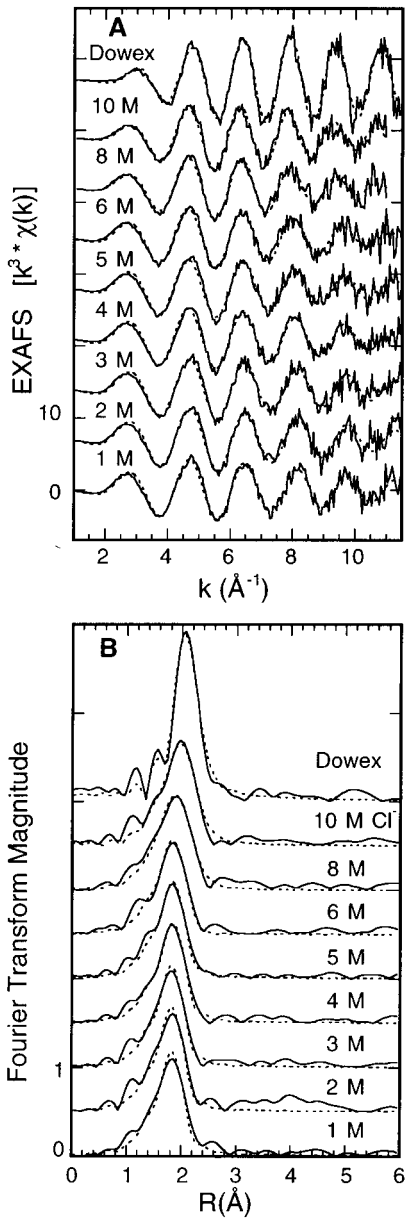


Figure 4. Raw Np L_{III}-edge k^3-weighted EXAFS data (A) and corresponding Fourier transforms (B) taken over $k = 1-11.5$ Å^{-1} for Np^{4+} as a function of [Cl^-] and the Np^{4+}/Dowex reference: experimental data (—); theoretical fit (···).

as well as a broadening in the FT peak. Since the origin of these changes was determined by curve fitting to be replacement of O by Cl^- in the coordination sphere (i.e., changes in N_O and N_{Cl^-}), the values of σ were fixed to those obtained from the $Np(H_2O)_{11}^{4+}$ and $NpCl_6^{2-}$ fits.

As described earlier, the 95% confidence limits for N and the F value ratios were evaluated to justify the inclusion of Cl^- (or O) in the fit.[35] Going from 5 to 10 M Cl^-, the curve fits demonstrate a systematic replacement of O by Cl^-. As the Cl^- concentration increases, N_{Cl^-} increases from 0 to 2.0 and N_O decreases from 10.3 to 7.7. Since the level of fit improvement increases from 5 to 10 M Cl^- and the 95% confidence level for N_{Cl^-} is ±0.36, the value of $N_{Cl^-} = 0.6$ obtained for the 6 M data confirms the presence of Cl^- in the inner sphere at this concentration. These results represent an average of all possible species, and a value of $N_{Cl^-} \sim 2$ in 10 M Cl^- indicates that multichloro complexes are formed, i.e., $Np(H_2O)_xCl_y^{4-y}$, with $y \geq 2$. Additionally, the Np^{4+} data show the same structural effect observed in the actinyl chloride complexes in that the O neighbors from water molecules move out as Cl^- enters the first coordination sphere.

Table 4. EXAFS Structural Parameters for Np^{4+} Chloride Solutions[a,b]

sample Np^{4+}	Np−O		Np−Cl			
	R (Å)	N	R (Å)	N	ΔE_0 (eV)	F ratio
1 M HCl	2.40	11.2			−8.1	1.0
2 M HCl	2.40	10.9			−7.8	1.0
3 M HCl	2.41	10.7			−7.6	1.0
4 M HCl	2.41	10.8			−7.4	0.94
5 M HCl	2.41	10.3			−7.2	1.0
6 M HCl	2.42	9.8	2.71	0.6	−7.3	0.81
8 M HCl	2.43	8.7	2.69	1.2	−7.0	0.44
10 M HCl	2.44	7.7	2.69	2.0	−7.2	0.25
Dowex/HCl			2.61	6.1	−14.1	1.0
$[Np(NO_3)_6^{2-}]^c$	2.51	12.0				
$[Pu(NO_3)_6^{2-}]^d$	2.49	12.0				
$[Pu(NO_3)_2(H_2O)_x^{2+}]^d$	2.41	11.1				
NpO_2^e	2.35	8				
$Cs_2UCl_6^f$			2.62	6		
$Cs_2PuCl_6^g$			2.62	6		

[a] The 95% confidence limits for R and N as estimated by EXAFSPAK: Np−O, $R \pm 0.012$ Å and $N \pm 1.1$; Np−Cl, $R \pm 0.009$ Å and $N \pm 0.36$, respectively. [b] Debye-Waller factor held constant for the shells; Np−O, $\sigma^2 = 0.0075$; Np−Cl, $\sigma^2 = 0.0040$. [c] XRD; ref 42. [d] EXAFS; ref 40. [e] XRD; ref 41. EXAFS data from the present study give 7.8 O at 2.35 Å. [f] XRD; ref 25. [g] XRD; ref 43.

Pu^{3+} EXAFS. In contrast to the behavior of the UO_2^{2+}, NpO_2^+, and Np^{4+} ions, Pu^{3+} showed no evidence for the formation of inner-sphere chloro complexes up to a Cl^- concentration of 12.3 M. The Pu L_{II}-edge EXAFS data presented in Figure 5 display a trend of decreasing amplitude with no shifts to higher R as a function of increasing Cl^- concentration. The curve-fitting results in Table 5 show that, in dilute Cl^-, the Pu^{3+} environment consists of ∼10 ±1 O at 2.51 Å. This result agrees well with the average first-shell Ln^{3+} coordination in $Pr(OH)_3$ and $Nd(NO_3)_3{\cdot}6H_2O$, which consist respectively of 9 O at 2.53 Å and 10 O at 2.56 Å.[44,45] In a previous study using EXAFS, Nd^{3+} was found to have 9.5 water molecules at 2.51 Å.[46] The Nd^{3+} hydration number determined by EXAFS falls well within the range of values (8−10 waters) obtained by other methods.[47] In 12.3 M Cl^-, the Pu^{3+} coordination is reduced to 6 O neighbors at 2.50 Å. The decrease in N_O reflects the diminished activity of water at 12.3 M LiCl where $\gamma_{H_2O} \sim 0.175$.[48]

UO_2^{2+}, NpO_2^+, Np^{4+}, and Pu^{3+} XANES. The XANES spectra provide another diagnostic tool for studying the changes in these solutions as a function of Cl^- concentration. Figure 6 shows representative L_{III}-edge spectra for UO_2^{2+}, NpO_2^+, and Np^{4+} and L_{II}-edge spectra for Pu^{3+} with varying amounts of Cl^- ligation as determined by EXAFS. Since the U, Np, and Pu data were calibrated against their respective $Ac^{IV}O_2$ powder XANES spectra (nearly identical),[49] the data in Figure 6 are displayed on a relative energy scale, which allows for direct comparison among the Np, U, and Pu spectra. The $L_{II,III}$ absorption edges of the actinides arise from the formally allowed $2p_{1/2,3/2} \rightarrow 6d$ electronic transitions, and changes in the L_{III} XANES for Ac(III), Ac(IV), AcO_2^+, and AcO_2^{2+} ions have been discussed in detail.[49−53] The $L_{II,III}$ XANES for Ac(III, IV)

(44) Mullica, D. F.; Milligan, W. O.; Beall, G. W. *J. Inorg. Nucl. Chem.* **1979**, *41*, 525.
(45) Rogers, D. J.; Taylor, N. J.; Toogood, G. E. *Acta Crystallogr.* **1983,** *C39*, 939.
(46) Yamaguchi, T.; Nomura, M.; Wakita, H.; Ohtaki, H. *J. Chem. Phys.* **1988**, *89*, 5153.
(47) Ohtaki, H.; Radnai, T. *Chem. Rev.* **1993**, *93*, 1157.
(48) Gazith, M. *Molal Osmotic Coefficients and Water Activities for Various Electrolytes*; Report IA-1009; Israel AEC: Tel Aviv, 1965.
(49) Kalkowski, G.; Kaindl, G.; Bertram, S.; Schmiester, G.; Rebizant, J.; Spirlet, J. C.; Vogt, O. *Solid State Commun.* **1987**, *64*, 193.
(50) Farges, F.; Ponader, C. W.; Calas, G.; Brown, G. E., Jr. *Geochim. Cosmochim. Acta* **1992**, *56*, 4205.

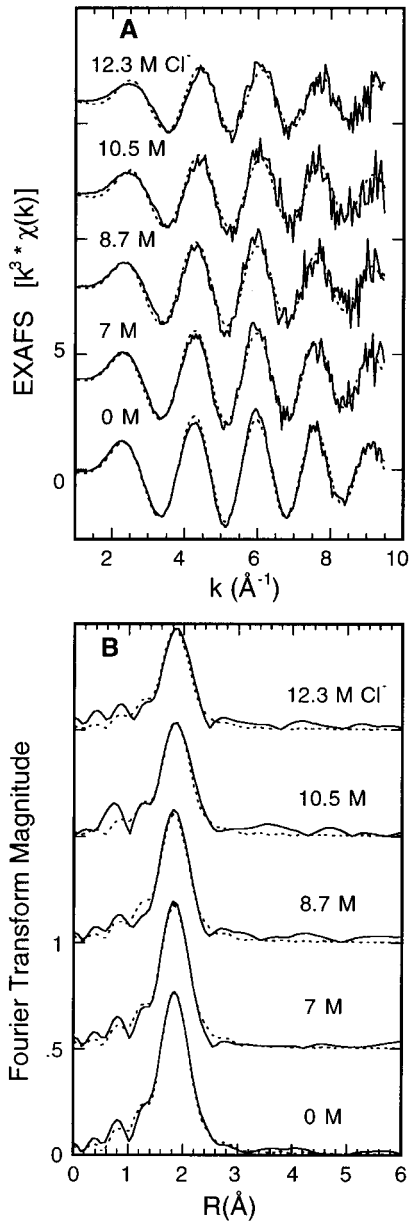


Figure 5. Raw Pu L_{II}-edge k^3-weighted EXAFS data (A) and corresponding Fourier transforms (B) taken over $k = 1-9.5$ Å^{-1} for Pu^{3+} as a function of [Cl^-]: experimental data (—); theoretical fit (···).

Table 5. EXAFS Structural Parameters for Pu^{3+} Chloride Solutions[a,b]

sample Pu^{3+}	Pu−O (Ln−O)			
	R (Å)	*N*	ΔE_0 (eV)	*F* ratio
0.01 M LiCl	2.51	10.2	−10.4	1.0
7.0 M LiCl	2.51	8.8	−10.6	1.0
8.7 M LiCl	2.51	7.9	−10.0	0.93
10.5 M LiCl	2.50	6.6	−8.2	1.0
12.3 M LiCl	2.50	5.8	−7.3	1.0
$Pr(OH)_3$[c]	2.53	9		
$Nd(NO_3)_3 \cdot 6H_2O$[d]	2.56	10		
$[Nd(H_2O)_x^{3+}]$[e]	2.51	9.5		

[a] The 95% confidence limits for *R* and *N* as estimated by EXAFSPAK: Pu−O, $R \pm 0.006$ Å and $N \pm 1.1$. [b] σ^2 held constant for Pu−O at 0.0100 Å^2. [c] XRD; ref 44. [d] XRD; ref 45. [e] EXAFS, ref 46.

compounds are characterized by a single, relatively intense absorption peak or "white line" whereas the XANES for actinyl compounds typically display a less intense absorption peak (relative to AcO_2) with an MS resonance occurring ∼15 eV past the main peak.

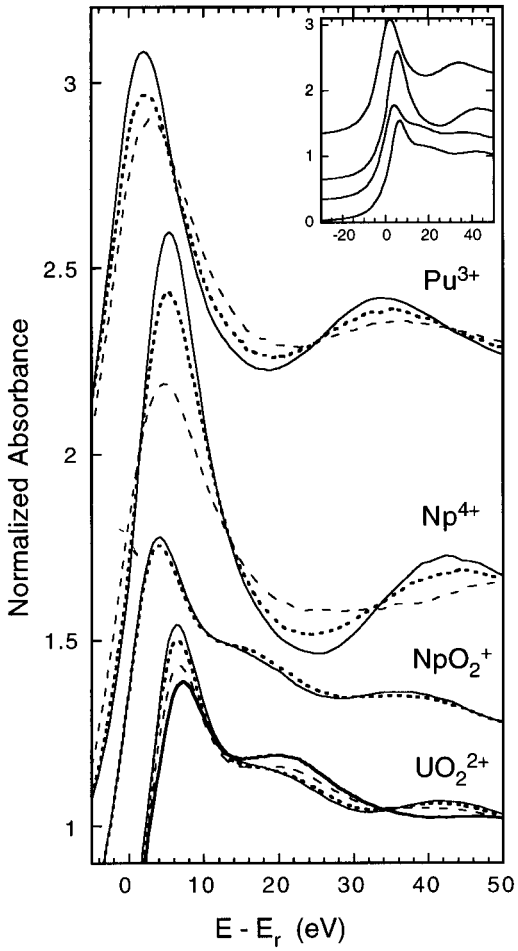


Figure 6. Normalized actinide $L_{II,III}$-edges. Spectra are presented for Pu^{3+} in 0.01 M LiCl (—), 8.7 M LiCl (···), and 12.3 M LiCl (---); Np^{4+} in 1.0 M HCl (—), 10 M HCl (···), and Dowex resin (---); NpO_2^+ in 3 M LiCl (—) and 10 M LiCl (···); and UO_2^{2+} in 0.0 M HCl (—), 4 M HCl (···), 10 M HCl (---), and Dowex resin (═). The U, Np, and Pu data are plotted on a relative energy scale as described in the text. The insert compares the full edges for the respective actinide aquo complexes.

A visual inspection of Figure 6 shows that the relative positions of the edges for the various oxidation states are in agreement with those shown previously for U and Np compounds.[52,53] There are positive energy shifts going from Pu^{3+} to Np^{4+} and from NpO_2^+ to UO_2^{2+}, reflecting an increase in relative binding energy associated with an increase in positive charge on the actinide ion. However, there appears to be a negative energy shift from Np^{4+} to NpO_2^+.[53] The shifts in white line (WL) positions for the aquo ions were determined using a peak deconvolution procedure similar to ones employed previously for actinide L_{III}-edges.[51−54] Relative to the WL positions of the $Ac^{IV}O_2$ reference samples, the aquo ion WL shifts are −3.9 eV for Pu^{3+},[55] +0.7 eV for Np^{4+}, −1.3 eV for NpO_2^+, and +1.4 eV for UO_2^{2+}. The negative WL shift observed upon

(51) Petiau, J.; Calas, G.; Petitmaire, D.; Bianconi, A.; Benfatto, M.; Marcelli, A. *Phys. Rev. B* **1986**, *34*, 7350.
(52) Kalkowski, G.; Kaindl, G.; Brewer, W. D.; Krone, W. *Phys. Rev. B* **1987**, *35*, 2667.
(53) Bertram, S.; Kaindl, G.; Jové, J.; Pagès, M.; Gal, J. *Phys. Rev. Lett.* **1989**, *63*, 2680.
(54) Edge fits were done using EXAFSPAK, which treats the main absorption peak and other resonances as pseudo-Voigt peaks (mixture of Lorenztian and Gaussian shapes) and the discontinuous edge step function as the integral of a pseudo-Voigt function. The Ac(III, IV) spectra were fit using one peak plus the step function, while the actinyl XANES fits included a second peak to fit the MS resonance.
(55) XANES measurements performed for the Pu^{3+} aquo ion at the L_{III}-edge gave a WL shift of −3.7 eV relative to PuO_2.

going from Np^{4+} to NpO_2^+ may result from a combination of structural[51] and electronic[53] effects, which can be difficult to distinguish from each other. For example, recent theoretical modeling using FEFF6 has shown that much of the structure associated with the L_{III} XANES of UO_2 and UO_2^{2+} including the MS resonance in UO_2^{2+} (previously interpreted as a split WL)[53] can be accurately modeled using SS and MS paths which contribute to the EXAFS portion, $\chi(k)$, of the total absorption, $\mu(E)$.[56−58] The anomalous WL shifts for the actinyl spectra relative to Np^{4+} may also reflect the diminished positive charge density on the Ac atoms in the actinyl groups that arises because of the close proximity of the axial oxygen atoms. Indeed, electronic structure simulations and thermodynamic measurements have determined effective charges of 2.2 on Np in NpO_2^+ and 3.2 on U in UO_2^{2+}.[59,60]

The effects of Cl^- replacement on the Np^{4+} XANES in Figure 6 are clearly observed. As N_{Cl^-} increases, the WL loses intensity, and the low-k EXAFS signal at ∼40 eV progressively changes its position and amplitude. For Pu^{3+}, a decrease in N_O without any Cl^- ligation causes a similar reduction in the WL intensity. Increasing the Cl^- ligation around UO_2^{2+} also results in a decreased WL intensity and increased absorption in the vicinity of the MS resonance above the edge. The NpO_2^+ XANES data show a trend analogous to that of UO_2^{2+}. The XANES data for NpO_2^+ in 10 M Cl^- and for UO_2^{2+} in 4 M Cl^- are shown in Figure 6 for direct comparison since their EXAFS curve fits gave the same structural result of $N_{O_{eq}} \sim 1$. Even though the changes in the NpO_2^+ XANES are relatively small, they occur in the same direction as those in the UO_2^{2+} XANES. Independent of any detailed theoretical models and spectral assignments, these spectra show dramatic sensitivity to changes in the local structure and help to corroborate the results obtained from the EXAFS analysis. Given that the signal to noise ratio is substantially larger in the XANES region relative to the EXAFS region, the enhanced XANES sensitivity should be useful for future work on more dilute systems where EXAFS data are unattainable.

Concluding Remarks

This work has directly measured the formation of chloro complexes with the actinide ions Pu^{3+}, Np^{4+}, NpO_2^+, and UO_2^{2+} and characterized the structural parameters associated with the O and Cl^- ligation in these systems using XAFS spectroscopy. On the basis of the Cl^- concentrations that were required to form monochloro complexes with each ion, the log β_1 values for the reaction $Ac^{x+} + Cl^- \leftrightarrow AcCl^{x-1}$, where Ac = Pu^{3+}, Np^{4+}, NpO_2^+, or UO_2^{2+}, should follow the trend $UO_2^{2+} > Np^{4+} \approx NpO_2^+ \gg Pu^{3+}$. It is further possible to estimate the formation quotients by viewing the behavior of N_{Cl^-} vs $[Cl^-]$ as a type of titration curve, where [ ] refers to the molarity. If we assume that monochloro complex formation is the principal process occurring early in the titration (i.e. $N_{Cl^-} < 1$), the EXAFS data will depict an average of the two species that are present. When $N_{Cl^-} = 0.5$, $[Ac^{x+}] = [AcCl^{x-1}]$ and $\beta_1 = 1/[Cl^-]$. This calculation gives log $\beta_1 = -0.48$, -0.78, and -0.85 for UO_2^{2+}, Np^{4+}, and NpO_2^+, respectively (95% limits are ±12%). These molar concentration equilibrium quotients apply only for the ionic strength and temperature[61] at which they were determined. If we wish to deal directly with activities, one simplified approach is to assume equal activities for Ac^{x+} and $AcCl^{x-1}$ species (or alternatively that their activities tend to compensate each other). Then it is possible to calculate an equilibrium constant which includes the Cl^- activity by using $\beta_1^0 = 1/a_{Cl^-} = 1/\gamma_{Cl^-}m_{Cl^-}$, where a_{Cl^-} is the activity, γ_{Cl^-} is the mean molal activity coefficient, and m_{Cl^-} is molality.[62] This correction gives log $\beta_1^0 = -0.65$, -1.47, and -1.65 for UO_2^{2+}, Np^{4+}, and NpO_2^+, respectively (95% limits are ±21%).

A comparison of the log β_1 and log β_1^0 values calculated here with those given earlier[9−19] shows that there is good agreement in the relative trend among the different ions. However, the values determined by EXAFS are significantly lower than those obtained in earlier measurements. The origin of these discrepancies is not clear. However, for formation constants determined by ion exchange chromatography, the EXAFS results described in this work show that the ion exchange medium dramatically alters the formation of chloride complexes. Thus, the species $UO_2Cl_4^{2-}$ and $NpCl_6^{2-}$ were observed to readily form within the Dowex resin but were not observed as principal species in the aqueous chloride solutions. Solvent extraction methods may suffer from similar perturbations since the actinide ions under study are in contact with an organic solvent and extractant and numerous assumptions have to be made regarding the behavior of the extractant and the distribution of species among the different phases. In fact, in a recent study on NpO_2^+ complexation with Cl^-, it was suggested that the chloro complex formation may be overestimated by solvent extraction methods when compared to visible/near-IR spectroscopic results.[14] In this case, the presence of outer-sphere complexation or ion pairs was proposed to explain the discrepancy. From the EXAFS results presented in this work, only inner-sphere complex formation was determined. Detection of outer-sphere Cl^- complexation by EXAFS should yield a substantially weaker signal due to the lack of direct bonding and the increased distance, yet recent EXAFS results on aqueous solutions of Cr(III) and Zn(II) have suggested that detection of outer-sphere O (∼4.0 Å) or Cl^- (∼4.3 Å) complexation is possible.[63] For solutions of $LaCl_3$, XRD indicates the presence of a $La(H_2O)_9Cl_2^+$ complex where the La−Cl interactions are outer-sphere at ∼5 Å.[64] Although the Fourier transforms in Figures 1, 2, 4, and 5 show no interactions at $R \geq 4$ Å, which would indicate the presence of ordered shells of more distant neighbors, this does not exclude the possibility of outer-sphere Cl^- complexation being present in these systems. Since the presence of 1−2 Cl^- ions at 5.0 Å is likely to be undetectable by EXAFS, measurements employing other scattering techniques such as large-angle X-ray scattering (LAXS) are needed to investigate these possibilities further.

Acknowledgment. This work was supported by the Director, Office of Energy Research, Office of Basic Energy Sciences, Chemical Sciences Division of the U.S. Department of Energy, under Contract No. DE-AC03-76SF00098. This work was done (partially) at SSRL, which is operated by the Department of Energy, Division of Chemical Sciences. The authors also acknowledge the efforts of the EH&S personnel from LBNL, SLAC, and SSRL.

IC970502M

(56) Hudson, E. A.; Rehr, J. J.; Bucher, J. J. *Phys. Rev. B* **1995**, *52*, 13815.
(57) Allen, P. G.; Shuh, D. K.; Bucher, J. J.; Edelstein, N. M.; Palmer, C. E-A.; Marquez, L. N.; Hudson, E. A.; Silva, R. J.; Nguyen, S. N. *Radiochim. Acta* **1996**, *75*, 47.
(58) Hudson, E. A.; Allen, P. G.; Terminello, L. J.; Denecke, M.; Reich, T. *Phys. Rev. B* **1996**, *54*, 156.
(59) Denning, R. G. *Struct. Bonding* **1992**, *79*, 215.
(60) Choppin, G. R.; Rao, L. F. *Radiochim. Acta* **1984**, *75*, 47.
(61) The solution temperatures are estimated to be 25 ± 1 °C on the basis of readings taken periodically in the vicinity of the experimental hutch.
(62) Gazith, M. *Activity Coefficients of Various Electrolytes. Molal and Molar Concentrations;* Report IA-1004; Israel AEC: Tel Aviv, 1965.
(63) (a) Díaz-Moreno, S.; Muñoz-Páez, A.; Martínez, J. M.; Pappalardo, R. R.; Marcos, E. S. *J. Am Chem. Soc.* **1996**, *118*, 12654. (b) Muñoz-Páez, A.; Pappalardo, R. R.; Marcos, E. S. *J. Am Chem. Soc.* **1995**, *117*, 11710.
(64) Grigoriew, H.; Siekierski, S. *J. Phys. Chem.* **1993**, *97*, 5400.